Analysis of Suture Force Simulations for Optimal Orientation of Rhomboid Skin Flaps

Wenzhangzhi Guo[1,2,4(✉)] , Ty Trusty[2], Joel C. Davies[3], Vito Forte[4,5], Eitan Grinspun[2], and Lueder A. Kahrs[1,2,6,7]

[1] Medical Computer Vision and Robotics Lab,
University of Toronto, Toronto, ON, Canada
`wenzhi.guo@mail.utoronto.ca`
[2] Department of Computer Science, University of Toronto, Toronto, ON, Canada
[3] Department of Otolaryngology - Head and Neck Surgery, Sinai Health System,
University of Toronto, Toronto, ON, Canada
[4] The Wilfred and Joyce Posluns CIGITI,
The Hospital for Sick Children, Toronto, ON, Canada
[5] Department of Otolaryngology – Head and Neck Surgery,
University of Toronto, Toronto, ON, Canada
[6] Department of Mathematical and Computational Sciences,
University of Toronto Mississauga, Mississauga, ON, Canada
[7] Institute of Biomedical Engineering, University of Toronto, Toronto, ON, Canada

Abstract. Skin flap is a common technique used by surgeons to close the wound after the resection of a lesion. Careful planning of a skin flap procedure is essential for the most optimal functional and aesthetic outcome. However, currently surgical planning is mostly done based on surgeons' experience and preferences. In this paper, we introduce a finite element method (FEM) simulation that is used to make objective recommendations of the most optimal flap orientation. Rhomboid flap is chosen as the main flap type of interest because it is a very versatile flap. We focus on evaluating suture forces required to close a wound as large tension around it could lead to complications. We model the skin as an anisotropic material where we use a single direction to represent the course of relaxed skin tension lines (RSTLs). We conduct a thorough search by rotating the rhomboid flap in small increments ($1°$–$10°$) and find the orientation that minimizes the suture force. We repeat the setup with different material properties and the recommendation is compared with textbook knowledge. Our simulation is validated with minimal error in comparison with other existing simulations. Our simulation shows to minimize suture force, the existing textbook knowledge recommendation needs to be further rotated by $15°$–$20°$.

1   Introduction

Skin flap is a widely used technique to close the wound after the resection of a lesion. In a skin flap procedure, a healthy piece of tissue is harvested from a nearby site to cover the defect [1]. Careful planning of such procedure is often needed, especially in the facial region where aesthetic of the final outcome is crucial. The ideal wound closure is dependent on many factors including incision path, anisotropic skin tension, location with respect to aesthetic sub-units, and adjacent tissue types [1]. For each patient, there often exists many valid reconstructive plans and a surgeon needs to take the above factors into account to strive for the most optimal aesthetic result while making sure facial sub-units functionalities are not affected. While there are basic guidelines in medical textbooks, there is often no single recipe that a surgeon can follow to determine the most optimal surgical plan for all patients. Surgeons require a lot of training and experience before they can start to make such decisions. This poses a challenge as each surgeon has their own opinion on the best flap design for each case (so it is hard to reach a consensus) and training a new surgeon to perform this task remains difficult.

In this paper, we build a system to help surgeons pick the most optimal flap orientation. We focus on the rhomboid flap as it is a very versatile flap. According to medical textbooks [1,2], the course of Relaxed Skin Tension Lines (RSTLs) is important information for surgeons when deciding on the orientation of rhomboid flaps. We validate this claim with our simulation and provide new insights into designing rhomboid flaps. The main contributions of the paper are:

– We created a skin flap FEM simulation and validated the simulation outputs of rhomboid flaps against other simulators;
– We performed quantitative evaluation of the suture forces for rhomboid flaps and compared the result against textbook knowledge;
– We provided an objective and methodical way to make recommendations for aligning rhomboid flaps relative to RSTLs;
– We generated a database of rhomboid flap simulations under various material properties and relative angles to RSTLs.

2   Related Works

There exists various virtual surgical simulators for facial skin flap procedures. In a recent work, Wang and Sifakis et al. built an advanced skin flap simulator that allows users to construct free-form skin flaps on a 3D face model interactively [3] (We further reference this work as "UWG simulator"). Mitchell and Sifakis et al. also worked on earlier versions of interactive simulators where a novel computational pipeline was presented in GRIDiron [4] and an embedding framework

was introduced [5]. Additionally, there are also many other interactive tutorials created for educational purposes [6–8]. While the above simulators are all very valuable for surgical education, they do not provide recommendations for flap type or alignment.

To gain insights into deformations in a skin flap procedure, there are various FEM simulations with stress/strain analysis. Most of those simulations are built based on a commercial FEM software such as Abaqus [9–16], ANSYS [17–22], or MSC. Marc/Mentat [23,24]. In those simulations, one or more skin flap types are analyzed and visualizations of different stress/strain measures are provided. Stowers et al. [9] constructed a surrogate model for creating simulated result with different material properties efficiently. With this model, they ran simulations with various material properties of three different flaps (including rhomboid flap) and provided visualizations of strain distribution and optimal flap alignment with various material properties. However, they did not come up with a consistent conclusion for the most optimal alignment for rhomboid flap. Spagnoli et al. [10] and Rajabi et al. [20] both evaluated different internal angles of the rhomboid flap and provided recommendations for the most optimal design. Rajabi et al. [20] also provided a modified design for the rhomboid flap based on stress optimization. Rhomboid flaps were also analyzed for comparison between different age groups [13], for comparison between different skin models [17] and for analysis on 3D face models [19]. Although the above works all offer valuable insights, they do not provide recommendations for the most optimal orientation for rhomboid flap nor evaluation/comparison for their results.

3   Methods

We built our skin flap FEM simulation based on the open-source library Bartels [25] and different components of the simulation are described in this section.

3.1   Constitutive Model of Skin

The skin patch is modelled as a thin membrane that resides in two dimensional space (planar stress formulation), as it is a common setup in the existing literature [9–12]. We model the skin using the adapted artery strain energy model proposed by Gasser-Ogden-Holzapfel (GOH) [26]. The strain energy density function is the sum of a volumetric component (Ψ^{vol}), an isochoric component ($\bar{\Psi}^{iso}$) and an anisotropic component ($\bar{\Psi}^{f}$):

$$\Psi = \Psi^{vol} + \bar{\Psi}^{iso} + \bar{\Psi}^{f}. \tag{1}$$

The isochoric component is proportional to μ, the shear modulus and the anisotropic component is parameterized by k_1 and k_2, which are stiffness parameters. More details of the skin constitutive model can be found in Stowers et al. [9].

3.2   Cutting and Suturing

Cutting is accomplished by duplicating vertices along the cutting line and re-meshing the local neighborhood to setup the correct connections with the duplicated vertices. This mechanism can run very efficiently and is sufficient for our setup since we always triangulate the mesh area based on the specific flap type so cutting can only happen on edges. An illustration of such mechanism is shown in the Supplementary Material.

The suture process is implemented by adding zero rest-length springs between vertices. Different stages of a rhomboid flap procedure is shown in Fig. 1b to d.

3.3   Triangulation

In our setup, we assume the lesion is within a circular area at the center of the patch. Similar to [9], for each flap type, a predefined template is used to build the geometric shape of the flap and the corresponding suture points are manually specified. To ensure the symmetry of the patch boundary, the vertices on the outer bounds of the circular patch are generated so that there is one vertex every $90°$ (i.e. at $0°$, $90°$, $180°$, and $270°$). Then the vertices in each quadrant are evenly spaced, and the number of vertices in each quadrant is the same (the exact number depends on the triangulation density and size of the patch). The triangulation is generated with the publicly available library Triangle [27,28]. An example triangulation for rhomboid flap can be seen in Fig. 1.
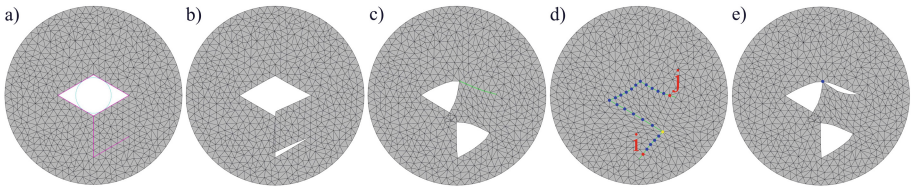

Fig. 1. FEM simulation of a rhomboid flap procedure. a) Initial setup for the rhomboid flap (flap design and cutting lines are shown in magenta and lesion is shown in cyan). b) Start of simulation. c) Completed suturing for one side (with green line representing the completed suture line). d) Completed procedure (colored dots indicate suture points). f) Example single-suture setup (the suture point is shown in blue). (Color figure online)

3.4   Validation

To validate our FEM simulation, we compared it with UWG simulator [3,29]. We first performed a skin flap procedure in UWG simulator and took a screenshot of the head model with the flap design ("pre-operative" image) and another one with the completed flap procedure ("post-operative" image). Then we aligned the flap design in our simulation with the "pre-operative" image taken from UWG simulator. Next, we ran our simulation and obtained the final suture line.

Lastly, we compared the suture line of our simulation with the "post-operative" image. We used normalized Hausdorff distance [30] (nHD) to quantify similarities between two suture lines, where Hausdorff distance is divided by the larger of the height and width of the bounding box of the suture line generated by UWG simulator (an illustration of the pipeline is shown in Fig. 2).

3.5   Suture Force Analysis

Multi-sutures. As excess force along the suture line can cause wound dehiscence and complications [9], the flap rotation angle that requires the lowest suture force should be the optimal orientation. For this experiment, we set the direction of RSTLs to be the horizontal direction. The initial pose of the flap was oriented with its first segment of the tail (the one that is connected to the rhomboid) perpendicular to RSTLs, as seen in Fig. 1a. To reduce the effect of fixed boundary, we set the radius of the patch to be 1 unit and the radius of the lesion to be 0.1 unit. To find the optimal alignment, we rotated the flap design counter-clockwisely in increment of $10°$. After we found the rotation angle with minimum suture force, we fine-tuned the result by searching between $-10°$ and $+10°$ of that minimum rotation angle at increments of $1°$. For each rotation, after reaching steady state, we took the maximum suture force among all the sutures shown as colored dots in Fig. 1d (see Algorithm 1 in Fig. 3).
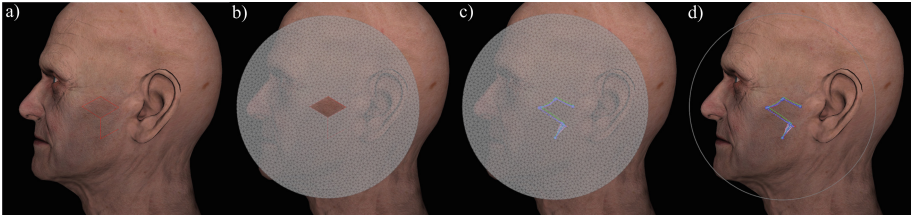

Fig. 2. Steps for comparing with UWG simulator output [3,29]. a) Flap design in UWG simulator. b) Mapping our simulation mesh to UWG simulator. c) Overlaying suture line generated by our simulation. d) Comparing our suture line with UWG simulator (our generated suture line is in green), $nHD = 0.0715$.

Algorithm 1 Multi-sutures
Require: All sutures are completed
$max\_force = 0$
$index = 1$
while $index <= j$ **do**
if $max\_force < suture\_force(index)$ **then**
$max\_force = suture\_force(index)$
end if
Increment $index$
end while
return max_force

Algorithm 2 Single-suture
$max\_force = 0$
$index = 1$
while $index <= j$ **do**
Complete suture at the current index
Set $current\_force$
if $max\_force < current\_force$ **then**
$max\_force = current\_force$
end if
Remove suture at the current index
Increment $index$
end while
return max_force

Fig. 3. Pseudocode of two different suture force analyses

To investigate the effect of material properties, we repeated the same procedure using the material properties listed in Table 1 (same range as in [9]). We changed one material property at a time while keeping other properties at the average (default) value. The material properties used in each trial can be seen in Table 1.

Table 1. Material properties of different trials (rows represent material parameters and columns represent trial setups). The ranges of valid material properties of the skin were taken from [9], where μ is the shear modulus, k_1 and k_2 are stiffness parameters.

	$default$	$small\_\mu$	$large\_\mu$	$small\_k_1$	$large\_k_1$	$small\_k_2$	$large\_k_2$
μ[kPa]	5.789	4.774	6.804	5.789	5.789	5.789	5.789
k_1[kPa]	106.550	106.550	106.550	3.800	209.300	106.550	106.550
k_2[−]	107.195	107.195	107.195	107.195	107.195	52.530	161.860

Single-suture. Instead of taking the maximum suture force after completing all sutures, we also experimented with making one suture at a time (see Algorithm 2 in Fig. 3) and picking the maximum suture force for any single suture (example of a single-suture step is shown in Fig. 1e).

4   Results

The simulation results were generated using a Macbook Pro and an iMac. It required around 30 s - 2 min to compute suture force for each rotation.

4.1   Validation with UWG Simulator

Further comparisons of skin flap placed at various locations of the face model are shown in Fig. 4. The normalized Hausdorff distances shown in Fig. 2 and 4 are all very small (below 0.1), indicating a good match between the two simulators.
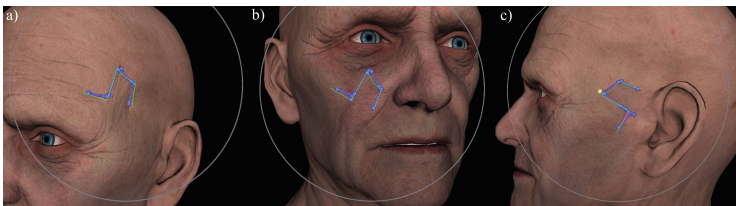

Fig. 4. Comparisons between our simulation and UWG simulator [3, 29] (our generated suture line is in green). a) Forehead ($nHD = 0.0893$). b) Cheek ($nHD = 0.0926$). c) Temple ($nHD = 0.0629$). (Color figure online)

4.2   Suture Force Analysis

Multi-sutures. The suture forces of various flap rotation angles under different material properties are shown in Table 2 and Fig. 5. Further analysis shows that the minimum suture force occurred at 99° and 281° (median value). As seen in Fig. 5b, the maximum force occurred at vertex 6 for all material properties (yellow dot in Fig. 1d), which is consistent with what is reported in literature [31].

Table 2. Optimal flap rotation angles (rows represent optimal configurations and columns represent trials of material properties presets).

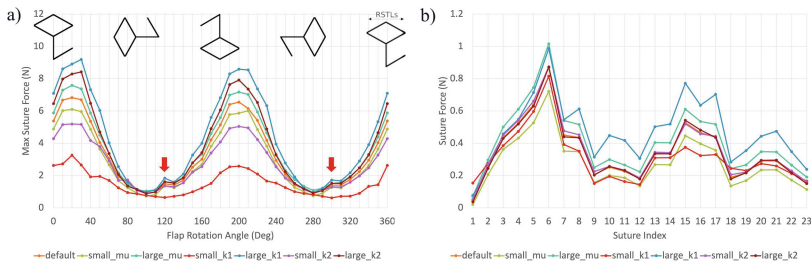|	$default$	$small\_\mu$	$large\_\mu$	$small\_k_1$	$large\_k_1$	$small\_k_2$	$large\_k_2$	**avg**	**med**
multi1 (deg)	99	103	99	127	100	99	99	104	99
multi2 (deg)	281	281	281	304	282	281	281	284	281
single1 (deg)	106	108	105	115	104	101	99	105	105
single2 (deg)	284	287	284	299	284	278	280	285	284

Fig. 5. Multi-sutures force visualization. a) Forces for various rotations (red arrows represent textbook recommendations). b) Suture force when rotation angle is at 99° (with default material properties); the suture index goes from i to j as shown in Fig. 1d. (Color figure online)

Single-suture. We repeated the same experiments with Algorithm 2 in Fig. 3 and the results are shown in Table 2 and Fig. 6. For our single-suture analysis, the minimum suture force occurred at 105° and 284° (median value).

4.3   Database Creation

While performing different experiments, we also created a dataset of rhomboid flap simulation videos under different material properties and the corresponding mesh at the end of each simulation. There are in total over 500 video clips of around 30 s. Overall, there are more than 10,000 frames available. A sample video can be found in the Supplementary Material. The dataset can be accessed through the project website: https://medcvr.utm.utoronto.ca/miccai2023-rhomboidflap.html.
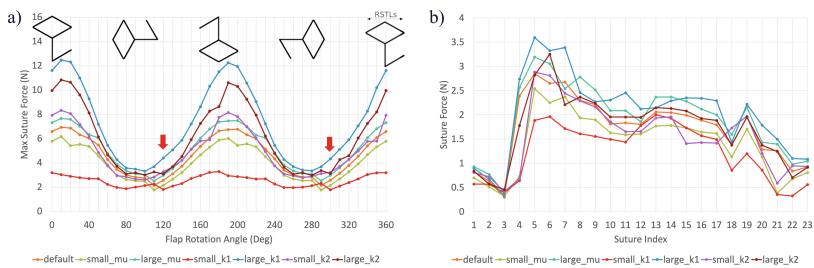
Fig. 6. Single-suture force visualization. a) Forces for various rotations (red arrows represent textbook recommendations). b) Suture force when rotation angle is at 89° (with default material properties); the suture index goes from i to j as shown in Fig. 1d. (Color figure online)
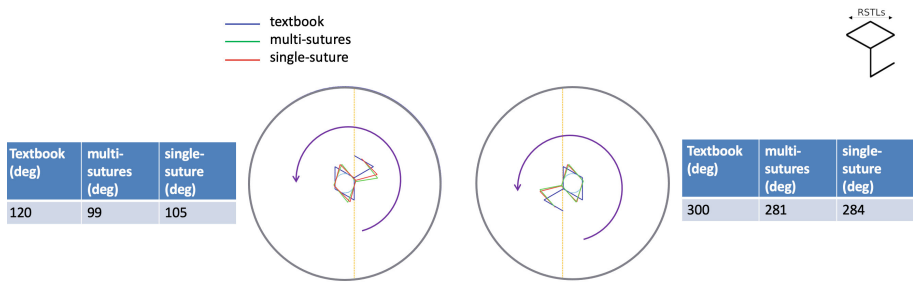

Fig. 7. Comparison between our suture force minimization result and textbook knowledge (yellow dotted line represents LMEs). (Color figure online)

5   Discussion and Conclusion

We built a FEM simulation to find the most optimal flap orientation for rhomboid flap based on suture force analysis. Through minimizing suture forces, we found that the optimal orientation occurred at 99°/281° and 105°/284° for multi-sutures and single-suture settings, respectively. The range of forces we obtained in our simulation is similar to what was reported in literature [22,24,32]. For Limberg flap (rhomboid flap with equal edge lengths and a top angle of 120°), there is a textbook description that aligns it based on lines of maximum skin extensibility (LMEs), which are perpendicular to RSTLs (see Supplementary Material). For our setting, this textbook alignment occurs at 120° and 300°. A comparison between our simulation and textbook knowledge is shown in Fig. 7.

Our experiment suggests that the minimal suture force occurs at a configuration that is close to textbook knowledge recommendation, but we found that rhomboid flaps have to be rotated further 15° to 20° away from the LMEs as seen in Fig. 7. This could be because that the textbook knowledge is trying to optimize a different goal or has taken other factors into account. Additionally, as

seen in Table 2, the optimal angle is consistent among all trials, except for trial $small\_k_1$ for both settings, which suggests that a good estimation of material properties of the patient's skin is needed before more specific recommendation of rhomboid flap orientation can be made.

Our current simulation does not take the complex physical structure of the human face into account. In this study, we aim to compare the prediction made by this setup with textbook knowledge based on RSTLs, which also does not take the more complex facial feature differences into account. This means our model will likely not work well on non-planar regions of the face. Further investigation and comparison with a physical setup (with either synthetic model or clinical setting) is also needed to show clinical significance of our result (for both suture forces comparison and flap orientation design). In the future, it would be interesting to continue investigating this topic by comparing behaviors of different flap types.

References

1. Baker, S.R.: Local Flaps in Facial Reconstruction, 2nd edn. Mosby, St. Louis (2007)
2. Weerda, H.: Reconstructive Facial Plastic Surgery: A Problem-solving Manual, 1st edn. Thieme, New York (2001)
3. Wang, Q., Tao, Y., Cutting, C., et al.: A computer based facial flaps simulator using projective dynamics. Comput. Methods Program. Biomed. **218**, 106730 (2022)
4. Mitchell, N., Cutting, C., Sifakis, E.: GRIDiron: an interactive authoring and cognitive training foundation for reconstructive plastic surgery procedures. ACM Trans. Graph. **34**(4), 1–12 (2015)
5. Sifakis, E., Hellrung, J., Teran, J., et al.: Local flaps: a real-time finite element based solution to the plastic surgery defect puzzle. Stud. Health Technol. Inform. **142**, 313–318 (2009)
6. Naveed, H., Hudson, R., Khatib, M., et al.: Basic skin surgery interactive simulation: system description and randomised educational trial. Adv. Simul. **3**(14), 1–9 (2018)
7. Shewaga, R., Knox, A., Ng, G., et al.: Z-DOC: a serious game for Z-plasty procedure training. Stud. Health Technol. Inform. **184**, 404–406 (2013)
8. Khatib, M., Hald, N., Brenton, H., et al.: Validation of open inguinal hernia repair simulation model: a randomized controlled educational trial. Am. J. Surg. **208**(2), 295–301 (2014)
9. Stowers, C., Lee, T., Bilionis, I., et al.: Improving reconstructive surgery design using Gaussian process surrogates to capture material behavior uncertainty. J. Mech. Behav. Biomed. Mater. **118**, 104340 (2021)

10. Spagnoli, A., Alberini, R., Raposio, E., et al.: Simulation and optimization of reconstructive surgery procedures on human skin. J. Mech. Behav. Biomed. Mater. **131**, 105215 (2022)
11. Alberini, R., Spagnoli, A., Terzano, M., et al.: Computational mechanical modeling of human skin for the simulation of reconstructive surgery procedures. Procedia Struct. Integr. **33**, 556–563 (2021)
12. Lee, T., Turin, S.Y., Stowers, C., et al.: Personalized computational models of tissue-rearrangement in the scalp predict the mechanical stress signature of rotation flaps. Cleft Palate Craniofac. J. **58**(4), 438–445 (2021)
13. Lee, T., Gosain, A.K., Bilionis, I., et al.: Predicting the effect of aging and defect size on the stress profiles of skin from advancement, rotation and transposition flap surgeries. J. Mech. Phys. Solids **125**, 572–590 (2019)
14. Lee, T., Turin, S.Y., Gosain, A.K., Bilionis, I., Buganza Tepole, A.: Propagation of material behavior uncertainty in a nonlinear finite element model of reconstructive surgery. Biomech. Model. Mechanobiol. **17**(6), 1857–1873 (2018). https://doi.org/10.1007/s10237-018-1061-4
15. Tepole, A.B., Gosain, A.K., Kuhl, E.: Computational modeling of skin: using stress profiles as predictor for tissue necrosis in reconstructive surgery. Comput. Struct. **143**, 32–39 (2014)
16. Flynn, C.: Finite element models of wound closure. J. Tissue Viab. **19**(4), 137–149 (2010)
17. Retel, V., Vescovo, P., Jacquet, E., et al.: Nonlinear model of skin mechanical behaviour analysis with finite element method. Skin Res. Technol. **7**(3), 152–158 (2001)
18. Pauchot, J., Remache, D., Chambert, J., et al.: Finite element analysis to determine stress fields at the apex of V-Y flaps. Eur. J. Plast. Surg. **36**, 185–190 (2012)
19. Kwan, Z., Khairu Najhan, N.N., Yau, Y.H., et al.: Anticipating local flaps closed-form solution on 3D face models using finite element method. Int. J. Numer. Method. Biomed. Eng. **36**(11), e3390 (2020)
20. Rajabi, A., Dolovich, A.T., Johnston, J.D.: From the rhombic transposition flap toward Z-plasty: an optimized design using the finite element method. J. Biomech. **48**(13), 3672–3678 (2015)
21. Remache, D., Chambert, J., Pauchot, J., et al.: Numerical analysis of the V-Y shaped advancement flap. Med. Eng. Phys. **37**(10), 987–994 (2015)
22. Topp, S.G., Lovald, S., Khraishi, T., et al.: Biomechanics of the rhombic transposition flap. Otolaryngol. Head Neck Surg. **151**(6), 952–959 (2014)
23. Yang, Z.L., Peng, Y.H., Yang, C. et al.: Preoperative evaluation of V-Y flap design based on computer-aided analysis. Comput. Math. Methods Med. 8723571 (2020)
24. Capek, L., Jacquet, E., Dzan, L., et al.: The analysis of forces needed for the suturing of elliptical skin wounds. Med. Biol. Eng. Comput. **50**(2), 193–198 (2012)
25. Bartels. https://github.com/dilevin/Bartels. Accessed 20 Feb 2023
26. Gasser, T.C., Ogden, R.W., Holzapfel, G.A.: Hyperelastic modelling of arterial layers with distributed collagen fibre orientations. J. R. Soc. Interface **3**(6), 15–35 (2006)
27. Shewchuk, J.R.: Triangle: engineering a 2D quality mesh generator and Delaunay triangulator. In: Lin, M.C., Manocha, D. (eds.) WACG 1996. LNCS, vol. 1148, pp. 203–222. Springer, Heidelberg (1996). https://doi.org/10.1007/BFb0014497
28. Jacobson, A., et al.: gptoolbox: geometry processing toolbox. http://github.com/alecjacobson/gptoolbox. Accessed 20 Feb 2023
29. SkinFlaps - a soft tissue surgical simulator using projective dynamics. https://github.com/uwgraphics/SkinFlaps. Accessed 10 Jan 2023

30. Huttenlocher, D.P., Klanderman, G.A., Rucklidge, W.J.: Comparing images using the Hausdorff distance. PAMI **15**(9), 850–863 (1993)
31. Borges, A.F.: Choosing the correct Limberg flap. Plast. Reconstr. Surg. **62**(4), 542–545 (1978)
32. Lear, W., Roybal, L.L., Kruzic, J.J.: Forces on sutures when closing excisional wounds using the rule of halve. Clin. Biomech. (Bristol Avon) **72**, 161–163 (2020)